APPLIED PHYSICS

p-type transparent superconductivity in a layered oxide

Takuto Soma[1], Kohei Yoshimatsu[1], Akira Ohtomo[1,2]*

Development of p-type transparent conducting materials has been a challenging issue. The known p-type transparent conductors unsatisfy both of high transparency and high conductivity nor exhibit superconductivity. Here, we report on epitaxial synthesis, excellent p-type transparent conductivity, and two-dimensional superconductivity of $Li_{1-x}NbO_2$. The $LiNbO_2$ epitaxial films with NbO_2 sheets parallel to (111) plane of cubic $MgAl_2O_4$ substrates were stabilized by heating amorphous films. The hole doping associated with Li^+ ion deintercalation triggered superconductivity below 4.2 kelvin. Optical measurements revealed that the averaged transmittance to the visible light of ~100-nanometer-thick $Li_{1-x}NbO_2$ was ~77%, despite the large number of hole carriers exceeding 10^{22} per cubic centimeter. These results indicate that $Li_{1-x}NbO_2$ is a previously unknown p-type transparent superconductor, in which strongly correlated electrons at the largely isolated Nb $4d_{z2}$ band play an important role for the high transparency.

INTRODUCTION

Search for new transparent conductors (TCs) is one of the most important subjects not only for practical use but also for advances in materials science (*1*). In case of n-type TCs, a variety of materials have been developed and used in industry. For example, Sn-doped In_2O_3 (ITO) exhibits high conductivity (~6000 S cm^{-1}) and high transparency (~80%) (*2*). Furthermore, even a transparent superconductor (TSC), which is regarded as an ultimate TC, was reported for $LiTi_2O_4$ epitaxial films (*3*). In contrast to n-type TCs, however, p-type TCs (p-TCs) are subjects of fundamental research since their performances are still low (*4*).

Zhang *et al.* (*5*) recently proposed new strategy for designing TCs based on transition-metal oxides (TMOs). In contrast to a traditional concept (taking ITO as an example, high-mobility semiconductor In_2O_3 is doped with a small amount of Sn), they shed light on correlated metals, where large number of carriers resides in low-mobility TMOs. On the basis of this strategy, perovskite-type AMO_3 (A = Ca, Sr, and La; M = V, Mo, and Cr) have been found to be good TCs, both n- and p-type (*5*–*8*). However, the studies have been so far limited to the perovskite-type TMOs. Thus, further investigation on other TMOs will pave a way for better p-TC performances.

To realize an excellent p-TC and p-type TSC (p-TSC), one may investigate two-dimensional materials, which have been enthusiastically studied in these days (*9*). Among various TMOs, we focus on a layered niobate, which is the only isostructural oxide to 2*H*-type transition-metal dichalcogenide (TMD) such as MoS_2 (*10*). The crystal structure of $LiNbO_2$ consists of NbO_6 triangular prisms (Fig. 1A), which are thought to create characteristic d-band splitting for realizing p-type conduction (*11*, *12*). Similar to TMDs, exotic properties can be expected (*13*, *14*). In addition, the wide bandgap nature of TMOs provides high transparency in the visible range (*15*). However, electronic properties of $LiNbO_2$ are still unclear. Although superconductivity was observed below 5 K in a Li-deficient phase $Li_{1-x}NbO_2$ ($x \sim 0.5$) (*16*), its electronic properties have not been investigated in detail (*17*). Moreover, there is no report about single-crystalline superconducting films, and their transport and optical properties are not yet fully understood.

Here, we fabricated superconducting $Li_{1-x}NbO_2$ epitaxial films using three-step synthesis method as illustrated in Fig. 1B and investigated their electronic properties. p-type doping associated with Li^+ ion deintercalation to $LiNbO_2$ triggered superconductivity and enhanced transparency in the visible range, and we created a p-TSC with strongly correlated electrons in two-dimensional NbO_2 conduction layers and isolated Nb $4d_{z2}$ band derived from the NbO_6 triangular prism coordination.

RESULTS

Three-step synthesis and structural properties

Figure 1C shows out-of-plane x-ray diffraction (XRD) profiles of Li-Nb-O films. The films prepared by the high-temperature direct growth (direct) showed 002 reflection of layered $LiNbO_2$ at $2\theta = 17.0°$ and a number of reflections from secondary phases, Li_3NbO_4 222, NbO_2 440, and $LiNbO_3$ 006 at $2\theta = 36.8°$, 37.3°, and 38.9°, respectively (*18*, *19*). The pulsed laser deposition (PLD) growth of Li-containing materials such as $LiCoO_2$ and $LiTi_2O_4$ often tends to form Li-deficient phases because Li atoms are easily scattered by gaseous species and/or reevaporated from the growing surface (*20*, *21*). In our case, however, the Li-rich phase (Li_3NbO_4) indicated much stronger peak than the Li-deficient phase (NbO_2) and stoichiometric phases ($LiNbO_2$ and $LiNbO_3$). The inclusion and unusual stability of Li_3NbO_4 were further verified by its excellent crystallinity irrespective of growth conditions (see section S1).

To avoid the formation of the secondary phases and to create layered $LiNbO_2$, we developed a three-step synthesis, which was initiated from PLD growth of Li-Nb-O films on the unheated substrates (step 1). Out-of-plane XRD profiles of the films at each step are also shown in Fig. 1C. In step 1, no film peak was observed, suggesting the amorphous phase. After in situ reductive annealing (step 2), clear 00*l* reflections of $LiNbO_2$ phase appeared without Li_3NbO_4 peaks despite the condition identical to the direct growth. A small peak of the oxidized phase ($LiNbO_3$) is thought to originate from partial oxidation of the $LiNbO_2$ phase. $LiNbO_3$ has wide bandgap and insulating nature and does not affect the transport and optical properties described below. Last, the $LiNbO_2$ films were immersed into an I_2/CH_3CN solution to deintercalate Li^+ ions

[1]Department of Chemical Science and Engineering, Tokyo Institute of Technology, 2-12-1 Ookayama, Meguro, Tokyo 152-8552, Japan. [2]Materials Research Center for Element Strategy (MCES), Tokyo Institute of Technology, Yokohama 226-8503, Japan. *Corresponding author. Email: aohtomo@apc.titech.ac.jp

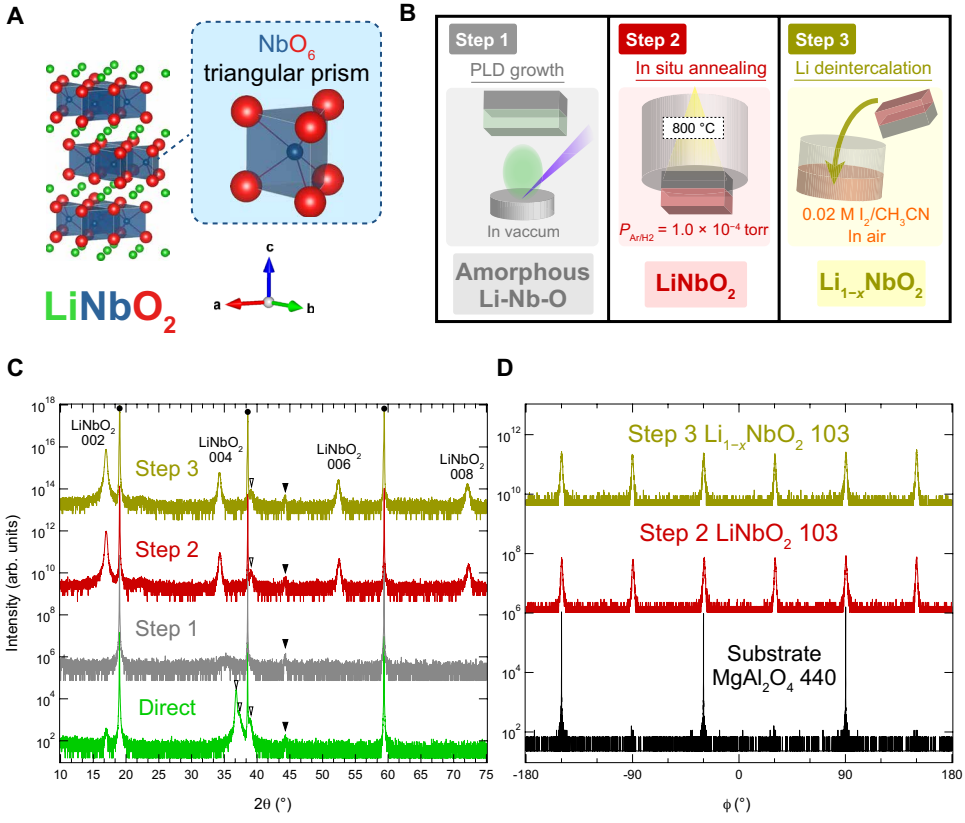

Fig. 1. Three-step synthesis method and structural analysis for $Li_{1-x}NbO_2$ epitaxial films. (**A**) Schematic crystal structure of $LiNbO_2$. The green, blue, and red spheres indicate lithium, niobium, and oxygen atoms, respectively. The magnified unit of NbO_6 takes a triangular prism structure. (**B**) Schematic illustrations of three-step synthesis method. The experimental conditions and produced compounds at each step are shown in each box. (**C**) Out-of-plane x-ray diffraction (XRD) profiles for the direct film and the films at each step. Filled circles indicate reflections coming from the $MgAl_2O_4$ substrates. Filled and open triangles indicate reflections coming from a sample stage and secondary phases, respectively. arb. units., arbitrary units. (**D**) XRD ϕ scans of reflections for $MgAl_2O_4$ 440 in the substrate, $LiNbO_2$ 103 in the step 2 film, and $Li_{1-x}NbO_2$ 103 in the step 3 film.

(step 3). This solution process is known to take place with the following redox reaction (*22*)

$$\text{Anodic reaction: } LiNbO_2 \rightarrow Li_{1-x}NbO_2 + x\,Li^+ + xe^- \quad (1)$$

$$\text{Cathodic reaction: } I_2 + 2e^- \rightarrow 2I^- \quad (2)$$

After the Li^+ ion deintercalation, only small shift of $LiNbO_2$ 00*l* peaks was observed, suggesting that NbO_2 layers in a host structure were preserved. Note that the crystallinity of the films (full width at half maximum of ω-scan profiles for $LiNbO_2$ 002 reflections) was unchanged.

We also measured asymmetric reflections (Fig. 1D). For both step 2 and step 3 films, the $LiNbO_2$ 103 reflection was clearly observed with a sixfold rotational symmetry, demonstrating solid-phase epitaxy at hexagonal planes (*10*). The angles of 440 reflections of the substrate coincided with those of the film, indicating an epitaxial relationship of $LiNbO_2$ [100] || $MgAl_2O_4$ <1$\bar{1}$0>. The lattice parameters for step 2 (step 3) films were calculated to be a = 2.906 (2.914) Å and c = 10.446 (10.468) Å. Bulk values of $Li_{0.93}NbO_2$ ($Li_{0.45}NbO_2$) were reported to be a = 2.906 (2.923) Å and c = 10.447 (10.455) Å (*16*), suggesting that the step 2 films had nearly stoichiometric composition, while the step 3 films had Li^+ ion deficiency. In addition, the in-plane lattice parameters at each step are considerably larger than that of $MgAl_2O_4$ ($d_{2\bar{2}0}$ = 2.858 Å), indicating unstrained film lattices.

Transport properties and strongly correlated electrons

The direct and step 1 films indicated resistivity (ρ) exceeding a measurement limit. Figure 2A shows the temperature dependence of ρ for the films at the following steps. The step 2 films showed ρ less than 10 milliohm·cm at 300 K and metallic conduction ($d\rho/dT > 0$). The step 2 films showed positive Hall coefficient, and hole concentration (n) was estimated to be 2.4×10^{21} cm^{-3} at 300 K (see section S2). On the other hand, decrease in ρ and change of the film color were found over the course of days, suggesting that oxidation upon exposure to air led to hole doping (*23*). To avoid any reaction in air, we prepared a capping layer (several-nanometer-thick amorphous alumina) before removing from the chamber (capped step 2). The capped step 2 films showed insulating behavior ($d\rho/dT < 0$) with higher ρ (50 milliohm·cm at 300 K) and lower n (6.4×10^{20} cm^{-3} at 300 K). Therefore, it is concluded that the metallic conduction in the step 2 films arises from easily oxidized (hole dopable) nature of $LiNbO_2$. It should be emphasized that the electronic ground state of $LiNbO_2$ has been controversial (*17*). Our results strongly suggest that $LiNbO_2$ is an insulator and supports a theoretical study (*24*).

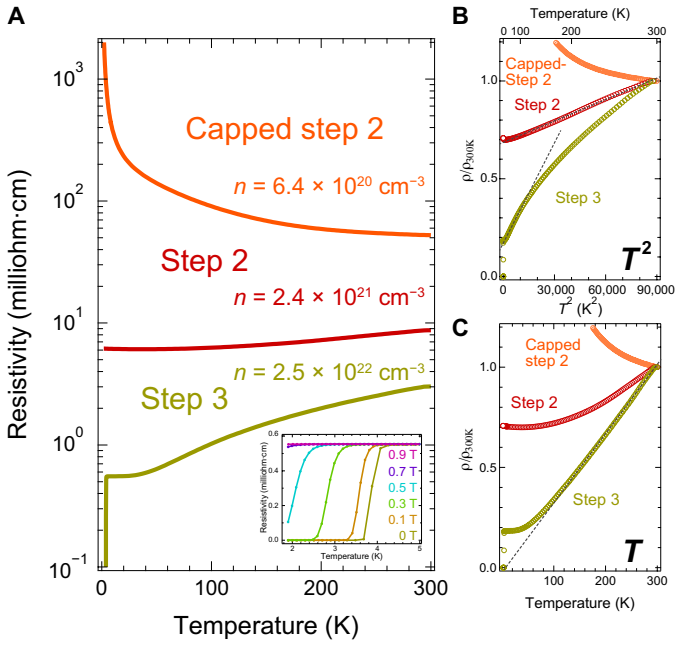

Fig. 2. Transport properties and Fermi-liquid analysis. (**A**) Temperature dependence of resistivity for the films at each step. The labeled values are hole concentration at 300 K (*n*) obtained by Hall measurements. Inset: Superconducting properties of the step 3 films. Magnification of that is indicated in the main panel, and its magnetic field (along the *c* axis) dependence was taken up to 0.9 T. (**B**) *T* and (**C**) T^2 dependence of ρ normalized by the values at 300 K for the films at each step. Dashed lines are linear fits to the plots.

The step 3 films showed much lower ρ (3 milliohm·cm at 300 K), higher *n* (2.5×10^{22} cm^{-3} at 300 K), and a superconductivity below 4.2 K, demonstrating superconducting transition in $Li_{1-x}NbO_2$ triggered by hole doping associated with the Li^+ ion deintercalation. Inset of Fig. 2A shows the magnification in the low-temperature range and modulation of superconductivity under magnetic field applied parallel to the *c* axis of $Li_{1-x}NbO_2$. The superconductivity was completely suppressed under a magnetic field as low as 0.9 T, which supports two-dimensional hole superconductivity in the NbO_2 plane (*25*). The critical magnetic field is much lower for a polycrystal (*26*). Moreover, superconductivity remained up to 4.2 T, when magnetic field applied perpendicular to the *c* axis, details of which will be published elsewhere. Further investigation on the two-dimensional hole superconductivity in our ideal samples is important, especially in connection with two-dimensional superconductors such as TMD and high–critical temperature (T_C) cuprate superconductors.

To elucidate how electron correlation works in $Li_{1-x}NbO_2$, we replot Fig. 2A for Fig. 2 (B and C), where the normalized resistivity (ρ/ρ_{300K}) is plotted as a function of *T* (Fig. 2B) and T^2 (Fig. 2C). A comparison between these plots allows us to elucidate a Fermi-liquid picture in the transport properties. We clearly demonstrate enhanced strength of electron correlation and non-Fermi liquid ground states in the superconducting $Li_{1-x}NbO_2$ films. We observed the linear T^2 dependence of ρ for the metallic step 2 and step 3 films, indicating Fermi-liquid ground states. However, their temperature ranges are different from one to another. The step 2 films showed good linearity lasting up to 300 K. In contrast, the step 3 films showed deviation from ~100 K and, instead, followed *T* linear dependence. This characteristic temperature, referred to as *T**, is regarded as an important phase point and/or a boundary in electronic phase diagrams of well-known cuprate, iron-pnictide superconductors, and heavy-fermion compounds (*27*, *28*). We find that, in our $Li_{1-x}NbO_2$, *T** showed a monotonic decrease by increasing the hole-doping level similar to well-established quantum critical systems, which we wish to publish elsewhere.

We performed fitting of T^2 plots to Fermi-liquid equation, i.e., $\rho = \rho_0 + AT^2$. We obtained $A = 3.3 \times 10^{-2}$ and 5.4×10^{-2} microhm·cm K^{-2} for step 2 and step 3 films, respectively. The *A* parameters are directly associated with effective mass of carrier *m** ($A \propto m^{*2}$). Conventional metals and metal-oxide conductors exhibit $A \sim 10^{-6}$ microhm·cm K^{-2} (*29*). On the other hand, strongly correlated metal oxides in the vicinity of Mott-Hubbard transitions (*30*) and heavy-fermion systems (*29*) show *A* in a range of 10^{-3} to 10 microhm·cm K^{-2}. The values obtained for our $Li_{1-x}NbO_2$ films are comparable to or larger than those of the latter, reflecting strong electron correlations. Apart from a class of metal oxides, electron correlations in $Li_{1-x}NbO_2$ are comparable to that in superconducting $Cu_{0.07}TiSe_2$, an intercalated TMDs (1.1×10^{-2} microhm·cm K^{-2}) (*31*). Furthermore, the roles of electron correlation in electronic structures of $Li_{1-x}NbO_2$ are also expected theoretically (*32*).

Optical properties and strongly isolated band structure

We have observed marked color changes throughout the three-step synthesis as shown in Fig. 3A. The direct and step 1 films indicated dark color typical of doped TMOs. In contrast, the step 2 films indicated characteristic bloody red, which is consistent with the previous

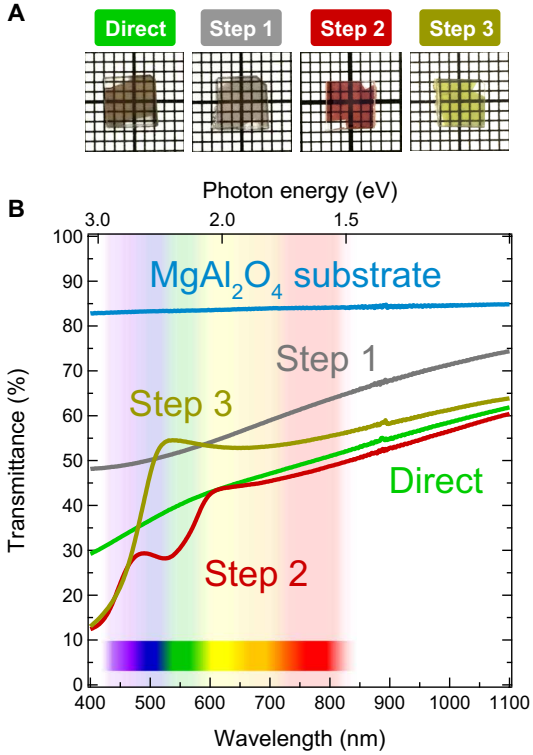

Fig. 3. Sample photographs and optical properties. (**A**) Optical images of the films at each step. Substrate size is about 5 mm by 5 mm. The transparent regions at the diagonal corners are trace of clamps that were used to hold the substrate to a metal backplate. (**B**) Optical transmittance spectra for the films at each step and $MgAl_2O_4$ substrate.

results (*27*). Furthermore, the step 3 films indicated transparent olive. Figure 3B shows optical transmittance in infrared to visible range for the films at each step and a pristine substrate. The first characteristic coloration in the step 2 films originated from drop of transmittance below 600 nm, which was consistent with calculated bandgap of layered $LiNbO_2$ (~2 eV) (*24*, *33*, *34*). The second color bleaching in the step 3 films resulted in increasing transmittance in the visible range. Unexpectedly, the average transmittance (T_{ave}) in the visible range (1.5 to 3.0 eV) reached ~50% despite a heavily hole-doped medium. Note that this value is the external transmittance, where substrate and light reflection at the surface and interface cause intensity loss. The T_{ave} after subtracting these contributions was as high as ~77%.

Taking difference between internal absorption spectra of $LiNbO_2$ and $Li_{1-x}NbO_2$ films into account, notable effects of the Li^+ ion deintercalation (hole doping) can be clearly captured (see section S3). The near–band edge absorption (2 to 2.5 eV) is greatly suppressed upon hole doping. In addition, the near-infrared absorption is hardly enhanced, although n increases by an order magnitude. The origin of this behavior will be explained later.

Performance as a p-TC

The p-TC performance of $Li_{1-x}NbO_2$ is summarized and compared with other p-TCs in Fig. 4, where their conductivities (σ) at room temperature (RT) are plotted as a function of T_{ave}. In general, σ and T_{ave} tend to indicate trade-off relationship as recently demonstrated in high-performance p-TCs of $La_{1-x}Sr_xCrO_3$ (LSCO) films. In this system, increase in x (number of holes) leads to increase in σ and decrease in T_{ave} (*8*). The lightly doped metallic $LiNbO_2$ (step 2) marks almost on the LSCO line. In contrast, the heavily doped superconducting $Li_{1-x}NbO_2$ marks beyond the border, highlighted by gradient background, and even violates the general tendency. Given the record large figure of merit as a p-TC and superconductivity, $Li_{1-x}NbO_2$ can be regarded the first p-TSC.

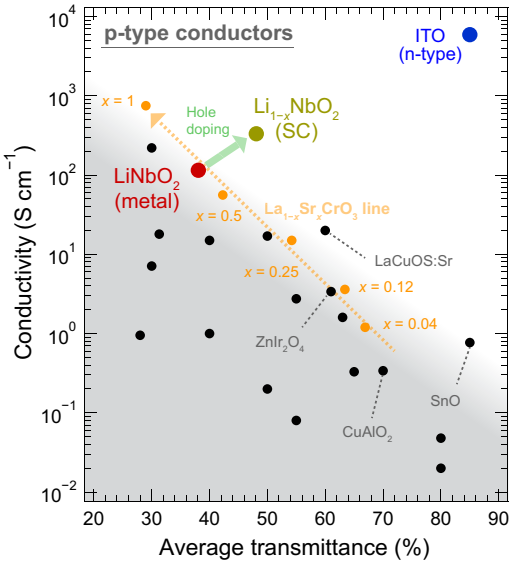

Fig. 4. Performances as a p-TC. Graphical representation of conductivity and transmittance for the $LiNbO_2$ (step 2) and $Li_{1-x}NbO_2$ (step 3) epitaxial films and reported p-TCs. Some of p-TCs are merely labeled, but all details including other p-TCs are listed in section S5. n-type ITO was also plotted as the ultimate performance for the purpose of exploring p-TCs. A series of LSCO, which is regarded as the guidance of TMO-based p-TC, was highlighted by a dashed arrow (*8*).

DISCUSSION

Let us explain the origin of the anomalous transparency of $Li_{1-x}NbO_2$. The degree of transparency in near-ultraviolet to near-infrared range can generally be divided into lower (near-infrared) and higher (near-ultraviolet) photon energy regime, which must be maintained against (i) free-carrier absorption, also known as a plasma reflection, and (ii) interband optical absorption, respectively (*5*). In conventional TCs, the higher σ becomes, the lower T_{ave} becomes due to (i). As for TMO-based TCs, T_{ave} can relatively be maintained against (i) due to large effective mass m^* of quasiparticle carriers. In contrast, $Li_{1-x}NbO_2$ rather harvests T_{ave} in terms of (ii) as will be explained as follows (schematically illustrated in Fig. 5).

Regarding (i), strongly correlated electrons decreased plasma reflection. Plasma energy ($\hbar\omega_p$) is associated with ratio of n to m^* (*5*). Our results allowed us to estimate m^* numerically, taking previously reported parameters into account (*24*). Suppose $\hbar\omega_p \sim 1$ eV for the step 3 films from decrease of transmittance in near-infrared region (Fig. 5), we obtain $m^* \sim 100\ m_0$ (see section S4). On the other hand, $\hbar\omega_p \sim 0.5$ eV was estimated for the step 2 films. The heavy mass is

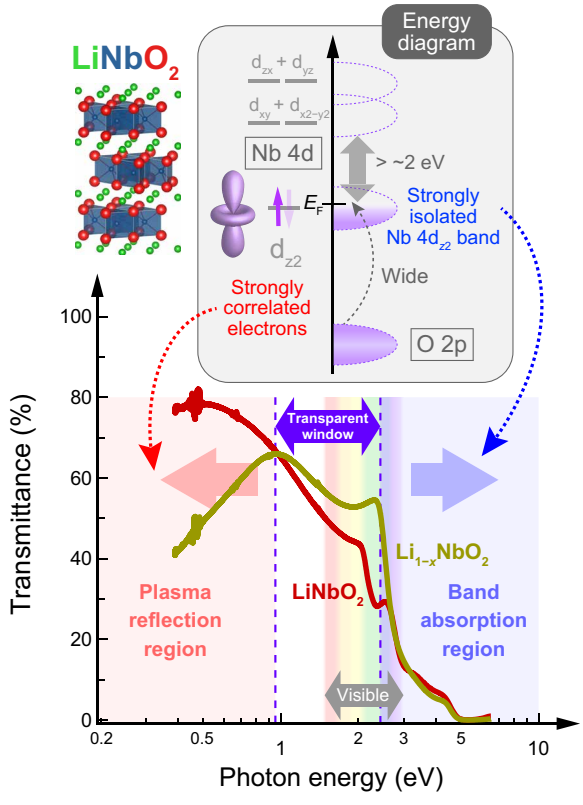

Fig. 5. Origins of p-type transparent superconductivity in $Li_{1-x}NbO_2$. Transmittance spectra in an extended range of photon energy and energy diagram of p-type transparent superconductivity in the $Li_{1-x}NbO_2$ epitaxial films. Strongly correlated electrons in $Li_{1-x}NbO_2$ decrease plasma energy. On the other hand, the strongly isolated Nb $4d_{z2}$ band located at E_F increases band absorption energy in each process. As a result, "transparent window" of $Li_{1-x}NbO_2$ becomes wider as almost comparable to visible range.

consistent with large A (3.3×10^{-2} and 5.4×10^{-2} microhm·cm K^{-2} for step 2 and step 3 films, respectively) described above. $Li_{1-x}NbO_2$ turned out to form strongly correlated electronic states, resulting in the lower $h\omega_p$ even when n exceeds 10^{22} cm^{-3}. Upon hole doping into $LiNbO_2$, $h\omega_p$ did not shift into the visible range. Thus, further carrier doping is acceptable to enhance the performance of p-TSC.

Regarding (ii), strongly isolated Nb $4d_{z2}$ band decreased interband optical absorption. According to our results and the reported band calculations, the Fermi level (E_F) was thought to locate in the band on Nb $4d_{z2}$ orbital, which was strongly isolated from the upper (degenerated Nb d_{xy} and d_{x2-y2} orbitals) and the lower (O 2p orbitals) bands. Note that highly isolated single band has a potential to create high density of states at E_F and strong electron correlation, both of which are favorable to superconductivity (*34*). The characteristic layered NbO_6 triangular prism structure derives this prominent nature (*24*) and leads to the anomalous transparency. According to Fig. 5, bandgap becomes wider as E_F drops with increasing n. This effect known as Burstein-Moss effect extends a short wavelength cutoff to blue range (*35*). Combining these two effects in $Li_{1-x}NbO_2$ realizes appropriate transparent window ranging from 1.0 to 2.4 eV. One expects to expand this window to violet upon further deintercalation of Li^+ ions. Synergetic increase in σ allows $Li_{1-x}NbO_2$ to approach to ITO (Fig. 4). The transmittance can also be improved by reducing film thickness.

In summary, we have first grown two-dimensional $Li_{1-x}NbO_2$ epitaxial films using specialized three-step synthesis method. The hole doping associating the Li^+ ion deintercalation substantially enhances visible-light transparency and leads to superconductivity. We conclude that strongly correlated electrons in the isolated Nb $4d_{z2}$ band realize the p-type transparent superconductivity in $Li_{1-x}NbO_2$. Our study demonstrates a new approach to creating high-performance TCs.

MATERIALS AND METHODS

Sample fabrication

Li-Nb-O films were grown on $MgAl_2O_4$ (111) substrates using PLD method with KrF excimer laser (1.0 J cm^{-2}). A Li excess ceramic ($Li_{1.2}NbO_{2+\delta}$) was prepared by conventional solid-state reaction steps, starting from mixing Li_2CO_3 and Nb_2O_5 powders with a molar ratio of 1.2:1. The direct growth was conducted at substrate temperature (T_s) of 800°C under a chamber pressure ($P_{Ar/H2}$) of 0.1 mtorr set by continues flow of Ar/H_2 (1 volume percent H_2) gas. The three-step synthesis method is illustrated in Fig. 1B. In step 1, using $Li_{1.2}NbO_{2+\delta}$ target, amorphous Li-Nb-O films were deposited in vacuum (background pressure, 1.0×10^{-7} torr) at RT. In step 2, Ar/H_2 gas was fed into the chamber to set $P_{Ar/H2}$ = 0.1 mtorr, and the step 1 films were annealed in situ at T_s = 800°C for 1 hour. In step 3, the step 2 films were exposed to air and immersed in 0.02 M I_2/CH_3CN solution for 15 min. Some films were capped by several-nanometer-thick alumina films using PLD at RT in vacuum for avoiding reactions with air (capped step 2).

Characterizations

Using a stylus profiler, film thickness was regulated to be ~100 nm. The crystal structures and epitaxial relationship were investigated by a laboratory XRD apparatus with Cu $K\alpha_1$ radiation. The temperature dependence of resistivity and the Hall voltage were measured by a standard four-probe method using a physical property measurement system (Quantum Design). The optical properties were investigated by ultraviolet-visible near-infrared spectroscopy at RT.

SUPPLEMENTARY MATERIALS

Supplementary material for this article is available at http://advances.sciencemag.org/cgi/content/full/6/29/eabb8570/DC1

REFERENCES AND NOTES

1. R. G. Gordon, Criteria for choosing transparent conductors. *MRS Bulletin* **25**, 52–57 (2000).
2. H. Ohta, M. Orita, M. Hirano, H. Tanji, H. Kawazoe, H. Hosono, Highly electrically conductive indium–tin–oxide thin films epitaxially grown on yttria-stabilized zirconia (100) by pulsed-laser deposition. *Appl. Phys. Lett.* **76**, 2740–2742 (2000).
3. A. Kumatani, T. Ohsawa, R. Shimizu, Y. Takagi, S. Shiraki, T. Hitosugi, Growth processes of lithium titanate thin films deposited by using pulsed laser deposition. *Appl. Phys. Lett.* **101**, 123103 (2012).
4. K. H. L. Zhang, K. Xi, M. G. Blamire, R. G. Egdell, *P*-type transparent conducting oxides. *J. Phys. Condens. Matter* **28**, 383002 (2016).
5. L. Zhang, Y. Zhou, L. Guo, W. Zhao, A. Barnes, H.-T. Zhang, C. Eaton, Y. Zheng, M. Brahlek, H. F. Haneef, N. J. Podraza, M. H. W. Chan, V. Gopalan, K. M. Rabe, R. Engel-Herbert, Correlated metals as transparent conductors. *Nat. Mater.* **15**, 204–211 (2016).
6. J. L. Stoner, P. A. E. Murgatroyd, M. O'Sullivan, M. S. Dyer, T. D. Manning, J. B. Claridge, M. J. Rosseinsky, J. Alaria, Chemical control of correlated metals as transparent conductors. *Adv. Funct. Mater.* **29**, 1808609 (2019).
7. L. Hu, R. Wei, J. Yan, D. Wang, X. Tang, X. Luo, W. Song, J. Dai, X. Zhu, C. Zhang, Y. Sun, $La_{2/3}Sr_{1/3}VO_3$ thin films: A new p-type transparent conducting oxide with very high figure of merit. *Adv. Electron. Mater.* **4**, 1700476 (2018).
8. K. H. L. Zhang, Y. Du, A. Papadogianni, O. Bierwagen, S. Sallis, L. F. J. Piper, M. E. Bowden, V. Shutthanandan, P. V. Sushko, S. A. Chambers, Perovskite Sr-doped $LaCrO_3$ as a new *p*-type transparent conducting oxide. *Adv. Mater.* **27**, 5191–5195 (2015).
9. Q. H. Wang, K. Kalantar-Zadeh, A. Kis, J. N. Coleman, M. S. Strano, Electronics and optoelectronics of two-dimensional transition metal dichalcogenides. *Nat. Nanotechnol.* **7**, 699–712 (2012).
10. G. Mayer, R. Hoppe, The first oxoniobate(III): $LiNbO_2$. *Angew. Chem. Int. Ed.* **13**, 744–745 (1974).
11. A. Miura, K. Tadanaga, E. Magome, C. Moriyoshi, Y. Kuroiwa, T. Takahiro, N. Kumada, Octahedral and trigonal-prismatic coordination preferences in Nb-, Mo-, Ta-, and W-based ABX_2 layered oxides, oxynitrides, and nitrides. *J. Solid State Chem.* **229**, 272–277 (2015).
12. N. Sarmadian, R. Saniz, B. Partoens, D. Lamoen, Easily doped *p*-type, low hole effective mass, transparent oxides. *Sci. Rep.* **6**, 20446 (2016).
13. C.-W. Chen, J. Choe, E. Morosan, Charge density waves in strongly correlated electron systems. *Rep. Prog. Phys.* **79**, 084505 (2016).
14. A. H. C. Neto, Charge density wave, superconductivity, and anomalous metallic behavior in 2D transition metal dichalcogenides. *Phys. Rev. Lett.* **86**, 4382–4385 (2001).
15. J. Shil, T. F. T. Cerqueira, W. Cui, F. Nogueira, S. Botti, M. A. L. Marques, High-throughput search of ternary chalcogenides for *p*-type transparent electrodes. *Sci. Rep.* **7**, 43179 (2017).
16. M. J. Gaselbracht, T. J. Richardson, A. M. Stacy, Superconductivity in the layered compound Li_xNbO_2. *Nature* **345**, 324–326 (1990).
17. E. G. Moshopoulou, P. Bordet, J. J. Capponi, Superstructure and superconductivity in $Li_{1-x}NbO_2$ ($x \approx 0.7$) single crystals. *Phys. Rev. B* **59**, 9590–9599 (1999).
18. A. Bartasyte, V. Plausinaitiene, A. Abrutis, S. Stanionyte, S. Margueron, P. Boulet, T. Kobata, Y. Uesu, J. Gleize, Identification of $LiNbO_3$, $LiNb_3O_8$ and Li_3NbO_4 phases in thin films synthesized with different deposition techniques by means of XRD and Raman spectroscopy. *J. Phys. Condens. Matter* **25**, 205901 (2013).
19. F. J. Wong, S. Ramanathan, Heteroepitaxy of distorted rutile-structure WO_2 and NbO_2 thin films. *J. Mater. Res.* **28**, 2555–2563 (2013).
20. T. Ohnishi, K. Takada, High-rate growth of high-crystallinity $LiCoO_2$ epitaxial thin films by pulsed laser deposition. *Appl. Phys. Express* **5**, 055502 (2012).
21. T. Oshima, K. Yokoyama, M. Niwa, A. Ohtomo, Pulsed-laser deposition of superconducting $LiTi_2O_4$ ultrathin films. *J. Cryst. Growth* **419**, 153–157 (2015).
22. H. Kuriyama, J. Matsuno, S. Niitaka, M. Uchida, D. Hashizume, A. Nakao, K. Sugimoto, H. Ohsumi, M. Takata, H. Takagi, Epitaxially stabilized iridium spinel oxide without cations in the tetrahedral site. *Appl. Phys. Lett.* **96**, 182103 (2010).
23. K. R. Dey, C. H. Rüscher, T. M. Gesing, A. Hussain, Phase transformation of lithium tungsten bronzes, Li_xWO_3, at room temperature ambient conditions. *Mater. Res. Bull.* **42**, 591–599 (2007).
24. E. R. Ylvisaker, W. E. Pickett, First-principles study of the electronic and vibrational properties of $LiNbO_2$. *Phys. Rev. B* **74**, 075104 (2006).

25. K. Ueno, T. Nojima, S. Yonezawa, M. Kawasaki, Y. Iwasa, Y. Maeno, Effective thickness of two-dimensional superconductivity in a tunable triangular quantum well of $SrTiO_3$. *Phys. Rev. B* **89**, 020508 (2014).
26. G. T. Liu, J. L. Luo, Z. Li, Y. Q. Guo, N. L. Wang, D. Jin, T. Xiang, Evidence of *s*-wave pairing symmetry in the layered superconductor $Li_{0.68}NbO_2$ from specific heat measurements. *Phys. Rev. B* **74**, 012504 (2006).
27. B. Keimer, S. A. Kivelson, M. R. Norman, S. Uchida, J. Zaanen, From quantum matter to high-temperature superconductivity in copper oxides. *Nature* **518**, 179–186 (2015).
28. J. G. Analytis, H.-H. Kuo, R. D. McDonald, M. Wartenbe, P. M. C. Rourke, N. E. Hussey, I. R. Fisher, Transport near a quantum critical point in $BaFe_2(As_{1-x}P_x)_2$. *Nat. Phys.* **10**, 194–197 (2014).
29. A. C. Jacko, J. O. Fjærestad, B. J. Powell, A unified explanation of the Kadowaki–Woods ratio in strongly correlated metals. *Nat. Phys.* **5**, 422–425 (2009).
30. N. E. Hussey, Non-generality of the Kadowaki–Woods ratio in correlated oxides. *J. Phys. Soc. Jpn.* **74**, 1107–1110 (2005).
31. E. Morosan, L. Li, N. P. Ong, R. J. Cava, Anisotropic properties of the layered superconductor $Cu_{0.07}TiSe_2$. *Phys. Rev. B* **75**, 104505 (2007).
32. K.-W. Lee, J. Kuneš, R. T. Scalettar, W. E. Pickett, Correlation effects in the triangular lattice single-band system Li_xNbO_2. *Phys. Rev. B* **76**, 144513 (2007).
33. X. Xu, G. Liu, S. Ni, J. T. S. Irvine, Layered lithium niobium (III) oxide—$LiNbO_2$ as a visible-light-driven photocatalyst for H_2 evolution. *J. Phys. Energy* **1**, 015001 (2019).
34. D. L. Novikov, V. A. Gubanov, V. G. Zubkov, A. J. Freeman, Electronic structure and electron-phonon interactions in layered Li_xNbO_2 and Na_xNbO_2. *Phys. Rev. B* **49**, 15830–15835 (1994).
35. Z. M. Gibbs, A. LaLonde, G. J. Snyder, Optical band gap and the Burstein–Moss effect in iodine doped PbTe using diffuse reflectance infrared Fourier transform spectroscopy. *New J. Phys.* **15**, 075020 (2013).
36. K. Fleischer, E. Norton, D. Mullarkey, D. Caffrey, I. V. Shvets, Quantifying the performance of *p*-type transparent conducting oxides by experimental methods. *Materials (Basel)* **10**, 1019–1122 (2017).
37. H. Sato, T. Minami, S. Takata, T. Yamada, Transparent conducting *p*-type NiO thin films prepared by magnetron sputtering. *Thin Solid Films* **236**, 27–31 (1993).
38. H. Kawazoe, M. Yasukawa, H. Hyodo, M. Kurita, H. Yanagi, H. Hosono, *p*-Type electrical conduction in transparent thin films of $CuAlO_2$. *Nature* **389**, 939–942 (1997).
39. A. Kudo, H. Yanagi, H. Hosono, H. Kawazoe, $SrCu_2O_2$: A *p*-type conductive oxide with wide band gap. *Appl. Phys. Lett.* **73**, 220–222 (1998).
40. H. Yanagi, S.-i. Inoue, K. Ueda, H. Kawazoe, H. Hosono, N. Hamada, Electronic structure and optoelectronic properties of transparent *p*-type conducting $CuAlO_2$. *J. Appl. Phys.* **88**, 4159–4163 (2000).
41. N. Duan, A. W. Sleight, M. K. Jayaraj, J. Tate, Transparent *p*-type conducting $CuScO_{2+x}$ films. *Appl. Phys. Lett.* **77**, 1325–1326 (2000).
42. K. Ueda, T. Hase, H. Yanagi, H. Kawazoe, H. Hosono, H. Ohta, M. Orita, M. Hirano, Epitaxial growth of transparent *p*-type conducting $CuGaO_2$ thin films on sapphire (001) substrates by pulsed laser deposition. *J. Appl. Phys.* **89**, 1790–1793 (2001).
43. R. Nagarajan, A. D. Draeseke, A. W. Sleight, J. Tate, *p*-type conductivity in $CuCr_{1-x}Mg_xO_2$ films and powders. *J. Appl. Phys.* **89**, 8022–8025 (2001).
44. M. K. Jayaraj, A. D. Draeseke, J. Tate, A. W. Sleight, *p*-type transparent thin films of $CuY_{1-x}Ca_xO_2$. *Thin Solid Films* **397**, 244–248 (2001).
45. J. Tate, M. K. Jayaraj, A. D. Draeseke, T. Ulbrich, A. W. Sleight, K. A. Vanaja, R. Nagarajan, J. F. Wager, R. L. Hoffman, *p*-type oxides for use in transparent diodes. *Thin Solid Films* **411**, 119–124 (2002).
46. H. Hiramatsu, K. Ueda, H. Ohta, M. Orita, M. Hirano, H. Hosono, Preparation of transparent *p*-type $(La_{1-x}Sr_xO)CuS$ thin films by r.f. sputtering technique. *Thin Solid Films* **411**, 125–128 (2002).
47. M. Dekkers, G. Rijnders, D. H. A. Blank, $ZnIr_2O_4$, a *p*-type transparent oxide semiconductor in the class of spinel zinc-d^6-transition metal oxide. *Appl. Phys. Lett.* **90**, 021903 (2007).
48. E. Fortunato, R. Barros, P. Barquinha, V. Figueiredo, S.-H. K. Park, C.-S. Hwang, R. Martins, Transparent *p*-type SnO_x thin film transistors produced by reactive rf magnetron sputtering followed by low temperature annealing. *Appl. Phys. Lett.* **97**, 052105 (2010).
49. M. Aksit, S. K. Kolli, I. M. Slauch, R. D. Robinson, Misfit layered $Ca_3Co_4O_9$ as a high figure of merit *p*-type transparent conducting oxide film through solution processing. *Appl. Phys. Lett.* **104**, 161901 (2014).
50. P. Zhai, Q. Yi, J. Jian, H. Wang, P. Song, C. Dong, X. Lu, Y. Sun, J. Zhao, X. Dai, Y. Lou, H. Yanga, G. Zou, Transparent *p*-type epitaxial thin films of nickel oxide. *Chem. Commun.* **50**, 1854–1856 (2014).
51. L. Farrell, K. Fleischer, D. Caffrey, D. Mullarkey, E. Norton, I. V. Shvets, Conducting mechanism in the epitaxial *p*-type transparent conducting oxide Cr_2O_3:Mg. *Phys. Rev. B* **91**, 125202 (2015).
52. A. Barnabé, Y. Thimont, M. Lalanne, L. Presmanes, P. Tailhades, *p*-type conducting transparent characteristics of delafossite Mg-doped $CuCrO_2$ thin films prepared by RF-sputtering. *J. Mater. Chem. C* **3**, 6012–6024 (2015).
53. J. Crêpellière, P. L. Popa, N. Bahlawane, R. Leturcq, F. Werner, S. Siebentritt, D. Lenoble, Transparent conductive $CuCrO_2$ thin films deposited by pulsed injection metal organic chemical vapor deposition: Up-scalable process technology for an improved transparency/conductivity trade-off. *J. Mater. Chem. C* **4**, 4278–4287 (2016).
54. R. Wei, X. Tang, L. Hu, J. Yang, X. Zhu, W. Song, J. Dai, X. Zhu, Y. Sun, Facile chemical solution synthesis of *p*-type delafossite Ag-based transparent conducting $AgCrO_2$ films in an open condition. *J. Mater. Chem. C* **5**, 1885–1892 (2017).

Acknowledgments

Funding: This work was partly supported by MEXT Elements Strategy Initiative to Form Core Research Center (grant no. JPMXP0112101001) and a Grant-in-Aid for Scientific Research (nos. 18H03925, 18 J10171, 19H02588, and 20K15169) from the Japan Society for the Promotion of Science Foundation. T.S. acknowledges the financial support from JSPS Research Fellowship for Young Scientists. **Author contributions:** T.S. performed the experiments and analyzed the experimental data. All authors discussed the results and wrote the manuscript. A.O. directed the project. **Competing interests:** The authors declare that they have no competing interests. **Data and materials availability:** All data needed to evaluate the conclusions in the paper are present in the paper and/or the Supplementary Materials. Additional data related to this paper may be requested from the authors.

Submitted 23 March 2020
Accepted 3 June 2020
Published 15 July 2020
10.1126/sciadv.abb8570

Citation: T. Soma, K. Yoshimatsu, A. Ohtomo, p-type transparent superconductivity in a layered oxide. *Sci. Adv.* **6**, eabb8570 (2020).

p-type transparent superconductivity in a layered oxide

Takuto Soma, Kohei Yoshimatsu and Akira Ohtomo

Sci Adv **6** (29), eabb8570.
DOI: 10.1126/sciadv.abb8570